SCIENCE PROGRESS

A rapid performance evaluation approach for lower mobility hybrid robot based on gravity-center position

Chensheng Wang[1,2], Fang Su[2], Yanqin Zhao[1], Hongda Liu[1], Yonghao Guo[1] and Wentie Niu[1,3]

[1]Key Laboratory of Modern Mechanisms and Equipment Design of the State Ministry of Education, Tianjin University, Tianjin, China
[2]School of Mechanical Engineering, Shanxi Datong University, Datong, China
[3]School of Mechanical Engineering, Tianjin University, Tianjin, China

Abstract

This article develops a rapid performance evaluation approach for lower mobility hybrid robot, which provides guidance for manipulator evaluation, design, and optimization. First, a general position vector model of gravity center for the lower mobility hybrid robot in the whole workspace is constructed based on a general inverse kinematic model. A performance evaluation index based on gravity-center position is then proposed, where the coordinates pointing to the supporting direction are selected as the evaluation index of the robot performance. Furthermore, the credibility of the evaluation approach is verified from a 5-DOF hybrid robot (TriMule) by comparing with the condition number and the first natural frequency. Analysis results demonstrate that the evaluation index can not only reflect the performance spatial distribution in the whole workspace but also is sensitive to the performance difference caused by mass distribution. The proposed performance evaluation approach provides a new index for the rapid design and optimization of the cantilever robot.

Keywords

Evaluation approach, gravity-center position, lower mobility, hybrid robot, evaluation index

Corresponding author:
Wentie Niu, School of Mechanical Engineering, Tianjin University, No. 135, Yagyuan Road, Jinnan District, Tianjin 300350, China.
Email: niuwentie@tju.edu.cn

Introduction

Hybrid robot has advantages of compact structure, high rigidity, and large bearing capacity, which has a broad application prospect in aerospace manufacturing, and in high-precision and high-intensity processing.[1–3] Performance evaluation is one of the key issues in robot design and application. It is of great significance to select the evaluation approaches and index, which could precisely constrain design variables in the design process and embody the real performance of robot in the application.[4,5]

At present, there are many evaluation approaches and indices for robot performance, including static structure symmetry, terminal stiffness, bearing capacity, force transfer, geometric accuracy, singularity, redundancy, and workspace, or dynamic precision, speed, dynamic stiffness, and mode shape.[6–9] Among them, the most typical evaluation indices of the local performance are the kinematic evaluation index based on the condition number (κ) of Jacobian matrix[10] and the dynamic stiffness evaluation index based on the low order natural frequency,[11] both of which are closely related to the specific pose of the robot. Salisbury and Craig[10] used the condition number as the evaluation index for the local performance of the robot. The smaller the condition number, the better the performance of the whole machine in this pose. Based on the Jacobian matrix, the problem of different physical quantities with different dimensions should be solved first, and then it should be normalized. Jacobian matrix depends on the pose of the robot, which is a local performance index. In order to evaluate the dexterity of robots in general, Gosselin and Angeles[12] proposed Global Conditioning Index. Huang et al.[13–15] applied this performance evaluation index to robot design, optimization, and evaluation. In the process of studying the performance of the robot, Dong et al.[16,17] and Wu et al.[18] assessed and evaluated its local performance with the help of the first natural frequency (f_1) of the robot. This approach has been widely used in the performance research and optimization design of various mechanisms. But acquisition of the first natural frequency of the mechanism mostly depends on the whole machine's numerical analytical dynamics model or finite element model. The accuracy of the model determines the reliability of the index. At present, most of the high-precision analytical models or finite element models have some errors, which limit the exploration of the real performance of the mechanism. The experimental method is the most accurate means to obtain the first natural frequency of the mechanism. However, as the complexity of the mechanism increases, the complexity of the experiment also increases, making it difficult to quickly evaluate and study the mechanism.

The position of gravity center has a significant impact on the performance of the robot in the whole workspace,[19–21] and gravity compensation has been a very important issue.[22–24] Wu et al.[25] studied the dynamic characteristics of the mechanism in consideration of gravity. Ma et al.,[26] in order to improve the performance of the robot, designed a barycenter balance mechanism to solve the influence caused by the barycenter in the process of work. As known to all, the gravity center of the mechanism is closely related to the pose of the robot. Moreover, the acquisition of

the gravity center is relatively simple, which only relies on the kinematics model and the fine 3D model. The gravity center has a high sensitivity to the difference of positions and orientations between the different poses. However, there is no systematic research on the relationship between the gravity-center position and the performance of the manipulator, even though the gravity-center position is introduced into the robot design and optimization.

In this article, a performance evaluation approach of the lower mobility hybrid robot based on the position of gravity center is presented, aiming to put forward a simple index which could be used for the rapid evaluation, design, and optimization of the robot. A general inverse kinematic model of the lower mobility hybrid robot is constructed, following a general position vector model of gravity center. Furthermore, the coordinates pointing to the supporting direction are selected as the performance evaluation index. The credibility of the evaluation approach is then verified from the 5-DOF hybrid robot (TriMule).

The remainder of the article is organized as follows. Section "Evaluation method based on gravity-center position" describes a general kinematics model and gravity-center position solution for the lower mobility hybrid robot. Thereafter, the evaluation index based on gravity-center position is established. In section "Performance evaluation of 5-DOF hybrid robot," the inverse kinematics solution model and the gravity-center vector model of the 5-DOF robot TriMule are deduced. Furthermore, the validity and reliability of the evaluation approach are verified by respectively comparing the gravity-center position with the condition number and the first natural frequency. Section "Application" discusses the selection of evaluation index based on the position of gravity center. Conclusions are made in last section.

Evaluation method based on gravity-center position

Kinematic analysis

The general model of a lower mobility hybrid robot is shown in Figure 1, which includes a fixed base, a moving platform, i limbs, and an end effector. One end of the limb is connected to the fixed base, and the other end is connected to the moving platform. It is customary to define the global coordinate frame *B-xyz* rigidly with the fixed base, and the moving coordinate frame *A-uvw* is fixed with the moving platform, and the cutter tool coordinate frame P' -$x_c y_c z_c$ is defined at the principal axis, respectively.

Then, the rotational transformation matrix of *A-uvw* with respect to *B-xyz* can be represented by R_A

$$R_A : \text{Trans}(A - uvw \to B - xyz) \tag{1}$$

The rotational transformation matrix of P' -$x_c y_c z_c$ relative to *A-xyz* can be expressed by R_C

$$R_C : \text{Trans}(P' - x_c y_c z_c \to A - uvw) \tag{2}$$
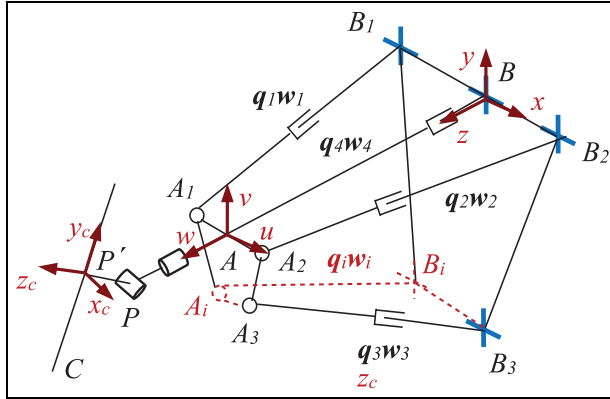
Figure 1. Schematic of the lower mobility hybrid robot.

The length and the direction vector of each limb or the rotational angle of end effector can be obtained through the inverse kinematic solution for the specific tool center point C.

Performance index based on gravity-center position

Based on the inverse kinematics model and the 3D model of the lower mobility hybrid robot, the parts are grouped according to the following principles:

1. The whole machine is grouped with joints as nodes;
2. When grouping, it is insisted that the relative position of the parts in the group does not change during the working;
3. The position vector of each part in *B-xyz, A-uvw*, or *P' -$x_c y_c z_c$* is easily obtained as a priority, because the direction vector of each limb and joint need to be deduced in the inverse kinematic model.

Assuming that the manipulator is divided into *i* components, the vector *i*th(*x, y, z*) in the specific coordinate frame and the mass can be checked in the 3D model according to the grouping. The corresponding transformation matrix $\boldsymbol{R}_i$ can be derived from the kinematic model. Then the vector of each gravity center in *B-xyz* can be expressed as

$$\boldsymbol{G}_i = \boldsymbol{R}_i \boldsymbol{j}(x, y, z) \tag{3}$$

Furthermore the gravity-center vector of the manipulator could be deduced as

$$\boldsymbol{G} = \frac{\sum\limits_{i=1}^{n} m_i \boldsymbol{G}_i}{\sum\limits_{i=1}^{n} m_n} \tag{4}$$
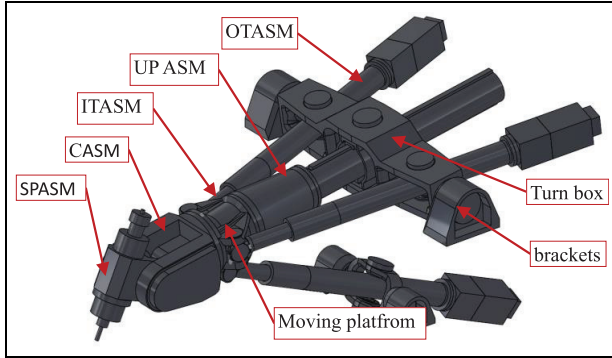
Figure 2. 3-D model of TriMule.

According to the cantilever direction of the mechanism, the evaluation index R_G is based on the position of the gravity center as

$$R_G = \left| G_{x/y/z} \right| \tag{5}$$

$R_G \geq 0$, and the larger the value, the greater the distance between the gravity center and the supporting surface, that is the worse the performance in the corresponding position.

Compared with other performance evaluation indices, such as κ and f_1, R_G is more intuitive, easier to obtain, and more operable. It is a convenient and rapid performance evaluation approach.

Performance evaluation of 5-DOF hybrid robot

The 5-DOF hybrid robot TriMule[27] is shown in Figure 2, which is composed of a spatial parallel module (3UPS&UP) and an A/C type wrist (2R) module attached to the moving platform. The 3UPS&UP consists of four limbs, wherein three active universal-prismatic-spherical (UPS) limbs have the same structure and are equally distributed within 360 degrees in space. One end of the UPS limb is connected to the rotational frame through universal joint, and the other end is connected to the moving platform through spherical joint. The passive universal-prismatic (UP) limb is arranged in the middle of limb 1 and limb 2, in which one end is connected to the fixed base by U joint, and the other section is consolidated with the moving platform. The 2R module is connected to the moving platform via a trust bearing, which has two rotational DOF, rotating along A-axis and C-axis, respectively.

According to the grouping principle mentioned in section 2, TriMule is grouped as UPS outer tubes assembly (OTASM), UPS limbs inner tubes assembly (INASM), UP assembly (UPASM), C-axis assembly (CASM), and A-axis assembly (SPASM).
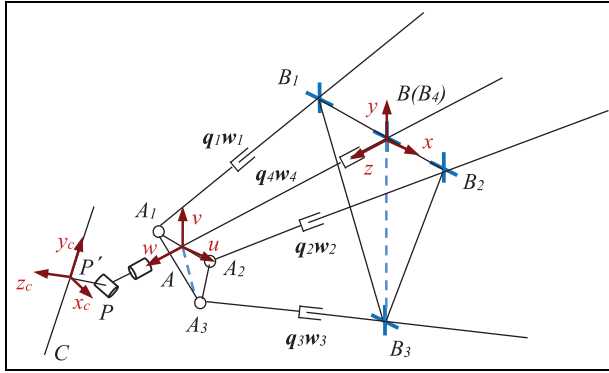
Figure 3. Schematic diagram of TriMule robot.

Kinematics analysis

Inverse kinematic model of the 3UPS&UP. The schematic of TriMule is shown in Figure 3. Herein, B_i is supporting point, and A_i is the junction between moving platform and the ith limb. A and B are the junctions of the UP limb with the moving platform and the rotational frame, respectively. Point P is the junction of C-axis rotational shaft and A-axis rotational shaft. P' is the intersection of spindle rotational shaft and C-axis rotational shaft. Point C is the tool center point.

The translational matrix R_A between the moving platform body and fixed coordinate frame (A-uvw) relative to the global coordinate frame (B-xyz) can be obtained through first rotating an angle ψ about the x-axis, then rotating an angle θ about v-axis, which can be expressed as

$$
\begin{aligned}
R_A &= \text{Rot}(x, \psi)\text{Rot}(v, \theta) \\
&= \begin{bmatrix}
\cos\theta & 0 & \sin\theta \\
\sin\psi\sin\theta & \cos\psi & -\sin\psi\cos\theta \\
-\cos\psi\sin\theta & \sin\psi & \cos\psi\cos\theta
\end{bmatrix}
\end{aligned}
\tag{6}
$$

The translational matrix R_C that P' -$x_c y_c z_c$ relative to A-xyz can be obtained through first rotating an angle δ about the w-axis, then rotating an angle β about u-axis, which can be represented as

$$
\begin{aligned}
R_C &= \text{Rot}(w, \delta)\text{Rot}(u, \beta) \\
&= \begin{bmatrix}
\cos\delta & -\sin\delta\cos\beta & \sin\delta\sin\beta \\
\sin\delta & \cos\delta\cos\beta & -\cos\delta\sin\beta \\
0 & \sin\beta & \cos\beta
\end{bmatrix}
\end{aligned}
\tag{7}
$$

If point A has been given, the inverse solution analysis of the 3-UPS&UP is equivalent to calculating the length and vector of each limb.

The position vector of point A in *B-xyz* can be calculated as

$$r_A = b_i + q_i w_i - a_i, \quad (i = 1, 2, 3) \tag{8}$$

$$r_A = q_4 w_4 \tag{9}$$

where, q_i represents the length of the ith limb, w_i represents the unit vector of the ith limb in *B-xyz*, q_4 represents the length of the UP limb, w_4 represents the unit vector of the UP limb in *B-xyz*, a_i represents the position vector of A_i in *A-uvw*, b_i represents the position vector of B_i in *B-xyz*.

The position vector of A_i in *A-uvw* can be calculated as

$$a_i = R a_{io} \tag{10}$$

$$a_{io} = a_i (\cos \gamma_i, \sin \gamma_i, 0)^T, \quad \gamma_i = \begin{cases} -\pi/2, & i = 1 \\ 0, & i = 2 \\ \pi, & i = 3 \end{cases} \tag{11}$$

Where, $a_i = \|AA_i\|$, γ_i is the angle between AA_2 and the *x*-axis.

The position vector of B_i in *B-xyz* can be expressed as

$$b_i = b_i (\cos \beta_i, \sin \beta_i, o)^T, \quad \gamma_i = \begin{cases} -\pi/2, & i = 1 \\ 0, & i = 2 \\ \pi, & i = 3 \end{cases} \tag{12}$$

Where, $b_i = \|BB_i\|$, γ_i is the angle between AA_2 and *x*-axis.

When $\psi = \theta = 0$

$$w_4 = R_A w = \begin{bmatrix} \sin \theta \\ - \sin \psi \cos \theta \\ \cos \psi \cos \theta \end{bmatrix} \tag{13}$$

$$w_4 = \frac{r_A}{q_4} = \frac{(x, y, z)^T}{\sqrt{x^2 + y^2 + z^2}} = \begin{bmatrix} S_{Ax} \\ S_{Ay} \\ S_{Az} \end{bmatrix}^T \tag{14}$$

Combining equations (13) and (14) yields

$$\theta = \arcsin(S_{Ax}), \psi = \arctan\left(-\frac{S_{Ay}}{S_{Az}}\right) \tag{15}$$

There is the transformation matrix R between *A-uvw* and *B-xyz*, and then substituting equation (15) into equations (8) and (9) leads to

$$q_i = |a_i - b_i + r_A| \quad w_i = \frac{(a_i - b_i + r_A)}{q_i} \tag{16}$$

Inverse kinematic solution of the 2R model. The position vector r_c of the tool center point C in *B-xyz* can be expressed as

$$r_C = l_C z_c + l_B y_c + r_p \tag{17}$$

$$r_p = (q_4 + l_A) w_4 \tag{18}$$

where $l_A = \|AP\|$, $l_B = \|PP'\|$, $l_C = \|P'C\|$, y_c represent the tool-axis vector, which can be derived through rotating δ about w-axis first, and then rotating β about u-axis

$$y_c = \mathrm{Rot}(y, \beta)\mathrm{Rot}(w, \delta)v = \begin{bmatrix} \cos\delta\sin\beta \\ -\sin\delta \\ \cos\delta\cos\beta \end{bmatrix} \tag{19}$$

One thing to point out is that tool-axis does not intersect with the A-axis. Therefore, in order to determine r_P from equation (17), it is necessary to determine z_c first. For a given r_c, construct the unit vector as

$$n = \frac{r_c}{|r_c|} \tag{20}$$

There u is perpendicular to the plane spanned by w and n, and when $|w \times n| \neq 0$, construct the unit vector as

$$u' = \pm \frac{w \times n}{|w \times n|}, \quad n = w \times u' \tag{21}$$

When $|w \times n| = 0$, w is collinear with n, u' has infinitely many solutions. Therefore, the robot is in a singular configuration. When $|w \times n| \neq 0$, u' has two solutions, the u' where $|r_P|$ is a smaller value should be adopted to obtain good kinematic performance and avoid mechanical interference.

So r_A can be expressed as

$$r_A = r_c - l_C z_c - l_B y_c - l_A w \tag{22}$$

Hence, taking norm on both sides of equation (18) leads to

$$q_4 = |r_P| - l_A, \quad w_4 = \frac{r_P}{q_4 + l_A} \tag{23}$$

Substituting equation (23) into equations (14)–(16), the rotational angle θ, ψ, the length q_i, and the unit vector w_i of the ith UPS can be obtained, respectively.

From $y_c = R_C R_A y$, $z_c = R_C R_A z$, there is

$$\begin{bmatrix} -\sin\delta\sin\beta \\ \cos\delta\sin\beta \\ \cos\beta \end{bmatrix} = R_C^T y_c = \begin{bmatrix} s_4 \\ s_5 \\ s_6 \end{bmatrix}, \quad \begin{bmatrix} \sin\delta\cos\beta \\ -\cos\delta\cos\beta \\ \sin\beta \end{bmatrix} = R_C^T z_c = \begin{bmatrix} s_7 \\ s_8 \\ s_9 \end{bmatrix} \tag{24}$$

According to equation (24), two rotational angles can be calculated

$$\beta = \arctan(s_9/s_6) \tag{25}$$

$$\delta = \begin{cases} \arctan{(-s_4/s_5)}, \beta \neq 0, \pi \\ \arctan{(-s_7/s_8)}, \beta = 0, \pi \end{cases} \tag{26}$$

Take an attention, when $\beta = \pi$, the robot is in the interference position

$$\delta = \arctan{(-s_4/s_5)}, \beta \neq \pi \tag{27}$$

Gravity-center position solution

Relative to the position vector of the tool center point C, the direction vector of the gravity center of the ith limb is the same as the vector w_i of the ith limb in the B-xyz. The gravity-center position of the limbs 1–3 OTASM in the B-xyz can be expressed as

$$\boldsymbol{G}_{wi} = \boldsymbol{R}_i \boldsymbol{q}_w - \boldsymbol{b}_i \ (i = 1, 2, 3) \tag{28}$$

where $\boldsymbol{q}_w$ represents the gravity-center vector of OTASM in U frame.

The gravity-center vector of INASM in the B-xyz can be expressed as

$$\boldsymbol{G}_{ni} = \boldsymbol{R}_i(\boldsymbol{q}_n + q_i \boldsymbol{w}_i) + \boldsymbol{r}_A \ (i = 1, 2, 3) \tag{29}$$

where $\boldsymbol{q}_n$ represents the gravity-center vector of INASM in S frame.

The gravity-center vector of UPASM in the B-xyz can be expressed as

$$\boldsymbol{G}_4 = \boldsymbol{R}_A \boldsymbol{q}_{G4} + \boldsymbol{r}_A \tag{30}$$

where $\boldsymbol{q}_{G4}$ represents the gravity-center vector of UPASM in A-uvw.

The mess of each assembly is expressed as m_{wi} (i = 1, 2, 3), m_{ni} (i = 1, 2, 3), m_4, respectively. The gravity-center vector $\boldsymbol{G_b}$ of the 3UPS&UP is derived as

$$\boldsymbol{G}_b = \frac{\sum\limits_{i=1}^{3} m_{wi} \boldsymbol{G}_{wi} + \sum\limits_{i=1}^{3} m_{ni} \boldsymbol{G}_{ni} + m_4 \boldsymbol{G}_4}{\sum\limits_{i=1}^{3} m_{wi} + \sum\limits_{i=1}^{3} m_{ni} + m_4} = \begin{bmatrix} G_{bx} \\ G_{by} \\ G_{bz} \end{bmatrix} \tag{31}$$

The whole mechanism is cantilever supported in the B-xyz. Therefore, the z-axis coordinate $\boldsymbol{G_b}$ is selected as the performance evaluation index of the 3UPS&UP

$$R_G = |G_{bz}| \tag{32}$$

The gravity-center position vector of the CASM in the B-xyz can be represented by

$$\boldsymbol{G}_A = \boldsymbol{R}_A \boldsymbol{q}_c + \boldsymbol{r}_A \tag{33}$$

Where, $\boldsymbol{q}_c$ represents the gravity-center vector of CASM in A-uvw.

The gravity-center position vector of the SPASM in the B-xyz can be expressed as

$$G_C = R_A(R_C(q_A + PP') + AP) + r_A \qquad (34)$$

where q_A represents the gravity-center vector of SPASM in P'-$x_c y_c z_c$.

The messes of CASM and SPASM are m_A, m_C, respectively. The gravity-center vector G_h of TriMule in the B-xyz is derived as

$$G_h = \frac{\sum_{i=1}^{3} m_{wi}G_{wi} + \sum_{i=1}^{3} m_{ni}G_{ni} + m_4 G_4 + m_A G_A + m_C G_C}{\sum_{i=1}^{3} m_{wi} + \sum_{i=1}^{3} m_{ni} + m_4 + m_A + m_C} = \begin{bmatrix} G_x \\ G_y \\ G_z \end{bmatrix} \qquad (35)$$

The whole mechanism is cantilever supported in the B-xyz. Therefore, the z-axis coordinate value G_h is selected as the performance evaluation index of the mechanism

$$R_G = |G_{hz}| \qquad (36)$$

Assembly parameters of TriMule are acquired by 3D model, as shown in Table 1. There are four things to add.

1. The length of U<u>P</u>S limb inner tubes assembly is 940×10^{-3} mm, in which gravity center away from S joint is 415.2×10^{-3} mm.
2. The distance between the spindle axis and the point A in moving platform is 342×10^{-3} mm.
3. $P'\,P = 120 \times 10^{-3}$ mm, the vector of point P in the A-uvw is $\{0, 0, 342 \times 10^{-3}$ mm$\}$, the vector of point C in P'-$x_c y_c z_c$ is $\{0, -320 \times 10^{-3}$ mm, $0\}$;
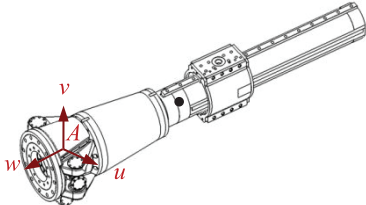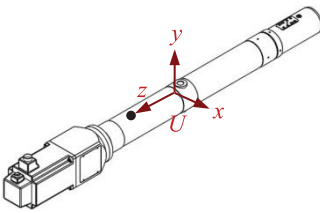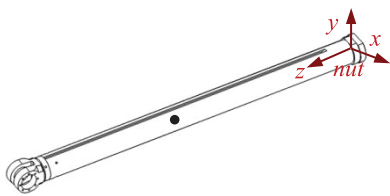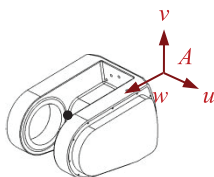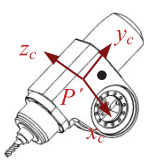4. The workspace of TriMule600: z = [600 mm:1200 mm], $x^2 + y^2 \leq 600^2$ mm.

Comparison with the kinematic index

The conditional number (κ) is an important evaluation approach for kinematics performance of manipulator. Literature[28] of the previous works analyzed kinematics performance of the 3U<u>P</u>S&UP of TriMule based on κ. In order to verify the validity of the gravity-center evaluation approach, two kinds of evaluation results of the 3U<u>P</u>S&UP were compared and analyzed in the same workspace. In addition, since many studies on TriMule have been carried out in published literature, its performance has a high consistency on the distribution rule in the whole workspaces. Herein, the gravity-center position index R_G is calculated within the plane of z = 800 mm plane, wherein $x^2 + y^2 \leq 600^2$ mm.

Figure 4(a) is the spatial distribution of κ, and Figure 4(b) is the spatial distribution of R_G. It can be seen from Figure 4 that κ and R_G have the same distribution trend within the plane of $z = 800$ mm.

Figure 5 shows the contour distribution of κ and R_G within the plane of z = 800 mm. As show in Figure 5(a), κ is symmetric about the x-axis and asymmetric about the y-axis. The minimum point of κ is (0, 0.04). It can be seen from Figure 5(b) that

Table 1. Assembly parameters.

Assembly	Gravity-center vector (mm)	Mess (kg)
	Vector in A-uvw; $\{x, y, z\}=\{-0.54, -4.03, -373.95\}$	96.316
	Vector in the U frame; $\{x, y, z\}=\{0.02, 0.46, -161.4\}$	34.412
	Vector in the nut frame; $\{x, y, z\}=\{0, 0, 524.8\}$	13.828
	Vector in the A-uvw; $\{x, y, z\}=\{45.44, -14.03, 194.58\}$	28.946
	Vector in the P' -$x_c y_c z_c$; $\{x, y, z\}=\{-8.94, -34.70, -18.63\}$	40.81

R_G is symmetric about the x-axis and asymmetric about the y-axis. The center of contour line distributions of R_G is lower than the y-axis, and the minimum point of R_G value is (0, 0.04). Furthermore, it is very clear that the two evaluation methods are highly consistent with the evaluation results of the 3UPS&UP.
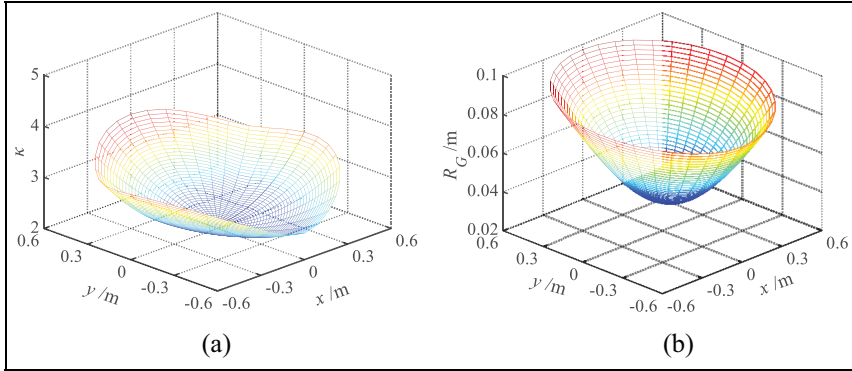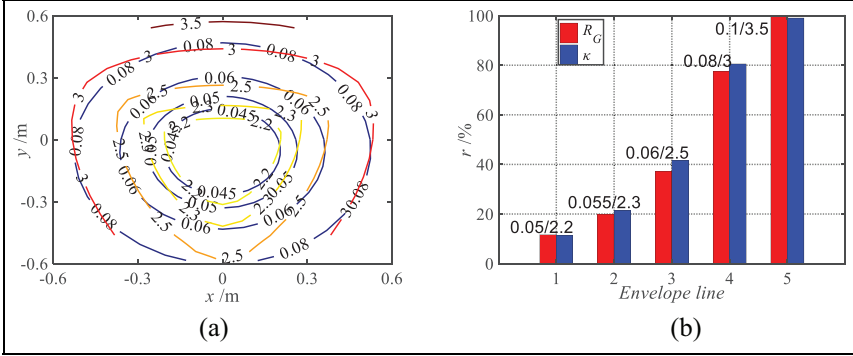
Figure 4. Distributions of κ and R_G within the plane of z = 0.8m: (a) spatial distribution of κ and (b) spatial distribution of R_G.
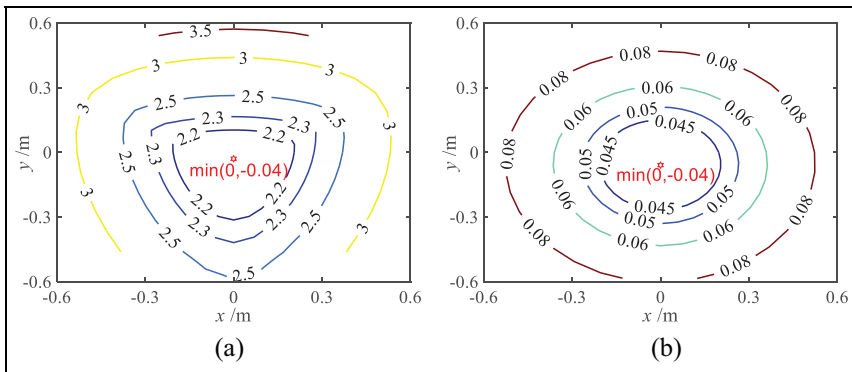

Figure 5. Contour line distributions of κ and R_G within the plane of z = 0.8 m: (a) contour line distributions of κ and (b) contour line distributions of R_G.

In order to further investigate the difference between the two evaluation approaches, the contour envelope area corresponding to the two evaluation approaches can be obtained through color filling, identification, and calculation. Figure 6(a) is the stacked diagram of the two evaluation indices, and Figure 6(b) is the proportion of contour envelope area corresponding to the two evaluation indices.

As shown in Figure 6(a), the contour line shapes of the two evaluation indicators are not the same, but the core areas covered by them are consistent and have good correspondence. That is to say, the optimal workspace based on the two indicators is same. In particular, Figure 6(b) shows that the two contour lines envelope areas that are almost equal, as the 0.05 of R_G corresponds to the 2.2 of κ, and the

Figure 6. Contour line distributions of κ and R_G of the plane z = 0.8: (a) contour line and (b) envelope area proportion statistics.
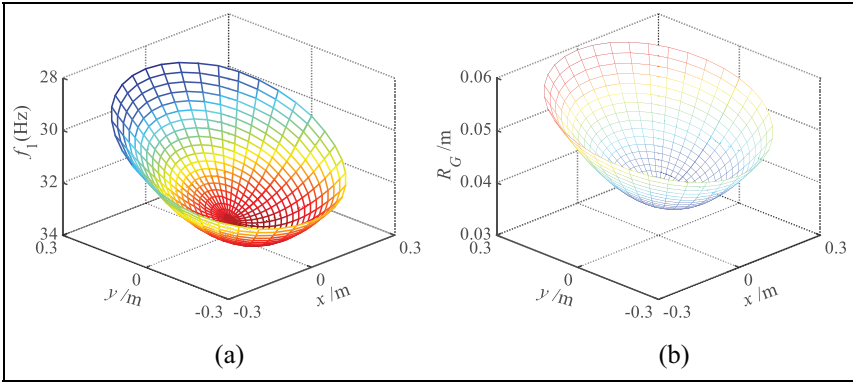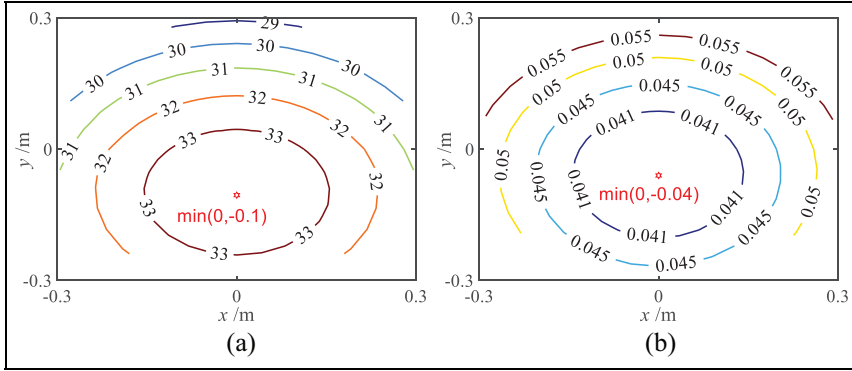

Figure 7. Spatial distributions of f_1 and R_G within the plane of z = 800 mm: (a) spatial distribution of f_1 and (b) spatial distribution of R_G.

0.055 of R_G corresponds to the 2.3 of κ, and so on, which finely demonstrates the consistency of the evaluation results of the two evaluation methods. Therefore, R_G is effective for the kinematics performance evaluation of the mechanism.

Comparison with the dynamic index

To further verify the validity of R_G, as mentioned earlier, z = 800 mm plane was selected for comparative analysis of R_G and the first-order natural frequency (f_1).[29]

Figure 7 compares f_1 from the previous works literature[29] and R_G for the 3UPS&UP, in the workspace of $x^2 + y^2 \leq 300^2$ mm. It can be seen that the spatial distribution of f_1 and R_G have the same distribution trend within the plane of z = 800 mm. Figure 7(a) is the spatial distribution of f_1, in which the direction of

Figure 8. Contour line distributions of κ and R_G within the plane of z = 0.8: (a) contour line distributions of κ and (b) contour line distributions of R_G.

z-axis is reverse for easy comparison, and Figure 7(b) is the spatial distribution of R_G, respectively.

Contour line distributions of f_1 and R_G within the plane of z = 800 mm as shown in Figure 8, where the shape of the two contour lines is ellipse. As show in Figure 8(a), f_1 is symmetric about the x-axis and asymmetric about the y-axis. The minimum point of κ is (0, 0.04), and the center of contour line distributions is lower than the y-axis. As shown in Figure 8(b), R_G is symmetric about the x-axis and asymmetric about the y-axis. The center of contour line distributions of R_G is lower than the y-axis, and the minimum point of R_G value is (0, 0.04). Therefore, it is very clear that the two evaluation methods are highly consistent with the evaluation results of the 3UPS&UP.

In order to further investigate the difference between the two evaluation approaches, the contour line envelope areas corresponding to the two evaluation approaches can be obtained through color filling and identification. Figure 9(a) is the stacked diagram of the two evaluation indices, and Figure 9(b) is the proportion of contour line envelope areas corresponding to the two evaluation indices.

Figure 9(a) shows the core areas covered by the contour line shapes of the two evaluation indicators are consistent. The results show the two evaluation indicators have a good correspondence. The difference is that the contour lines of f_1 have a certain displacement along the y-axis compared with the contour lines of R_G.

As shown in Figure 9(b), although there is a certain difference in 0.045 and 32, the overall contour line envelope areas are very consistent, which finely demonstrates the consistency of the evaluation results based on the two evaluation methods. All aforementioned proofs indicate the effectiveness of R_G on the performance evaluation for manipulator. From the foregoing analysis, κ, f_1, and R_G are consistent in the performance evaluation of cantilever robot. However, R_G is related to the dimensional parameters, and the quantitative expression of the relationship is related to the specific topology structure of the robot.
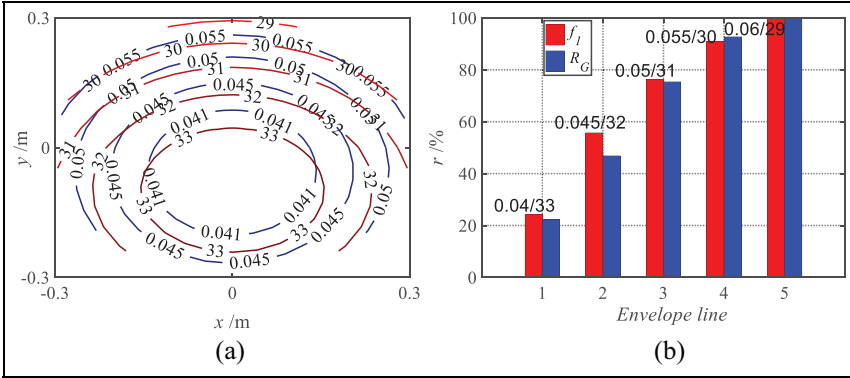
Figure 9. Contour lines distributions of κ and R_G of the plane z = 0.8: (a) contour lines and (b) envelope area proportion statistics.
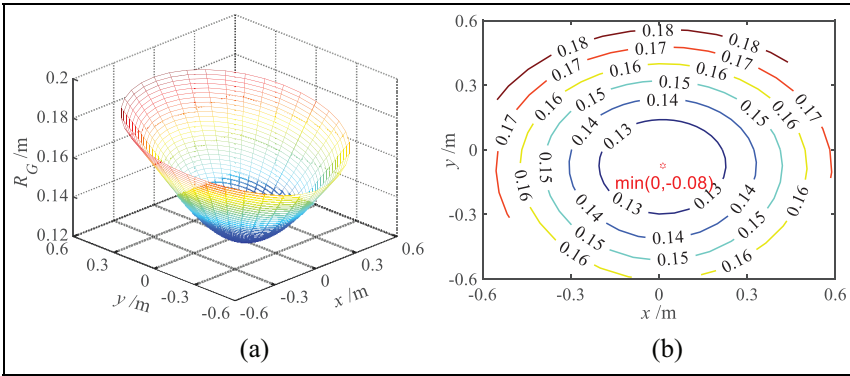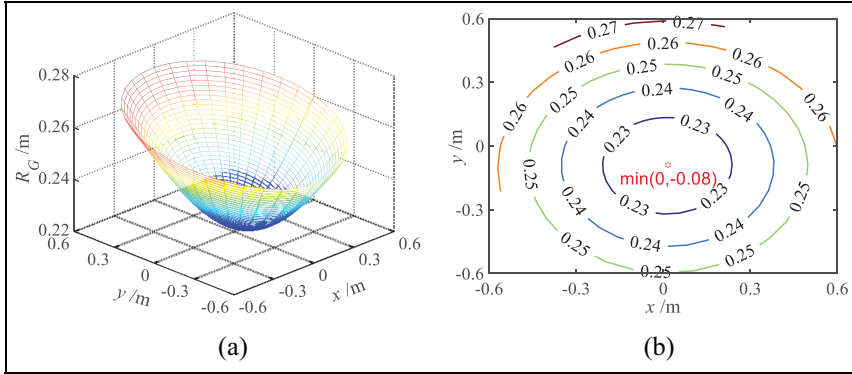

Figure 10. R_G distribution of TriMule within the plane of z = 600 mm: (a) spatial distribution and (b) contour lines.

Application

Analyses in the previous sections demonstrate enough credibility on R_G for cantilever robot. However, the most key problem is the determination of R_G in application. This requires enough research to establish corresponding relationship between the performance and R_G. The upper boundary of R_G is further determined, which is used for performance evaluation, design, and optimization.

The choice of R_G for performance evaluation

The gravity-center position of TriMule in whole workspace was analyzed. The results are shown in Figures 10–13, where z = 600 mm in Figure 10, z = 800 mm in

Figure 11. R_G distribution of TriMule within the plane of z = 800 mm: (a) spatial distribution and (b) contour lines.
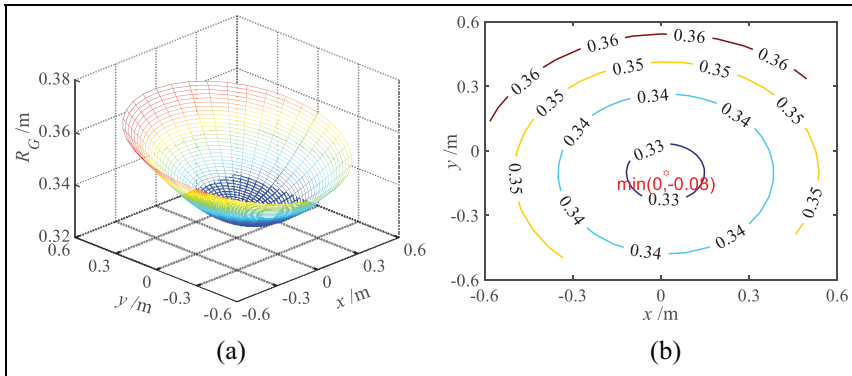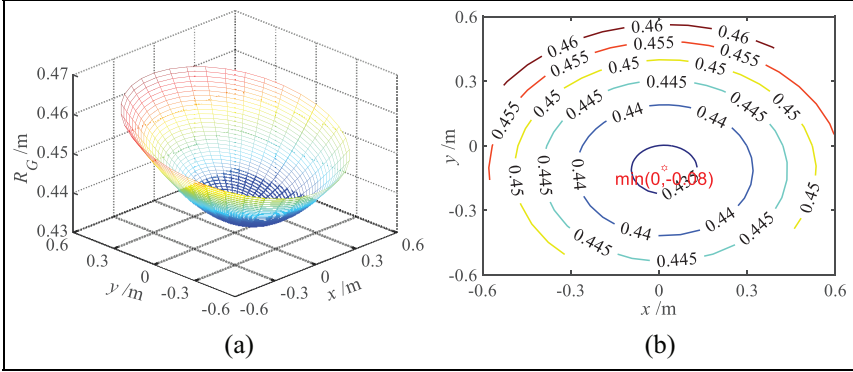

Figure 12. R_G distribution of TriMule within the plane of z = 1000 mm: (a) spatial distribution and (b) contour lines.

Figure 11, z = 1000 mm in Figure 12 and z = 1200 mm in Figure 13. In addition, (a) is the spatial distribution, and (b) is the corresponding contour distribution.

As shown in Figures 10–13, the distribution of R_G is not symmetry about x-axis in the whole workspace; moreover, the asymmetry increases as the z increases. The reason is that the mass distribution of 2R module is not symmetry about x-axis, which is bound to show that the performance of TriMule is not symmetry about x-axis in the whole workspace. Furthermore, the bigger z, the greater the impact on the performance of the distribution. However, κ and f_1 cannot accurately reflect the difference due to some simplification considerations in the modeling process.

In addition, Figures 10–13 show that the distribution of R_G in the whole workspace is very consistent. However, the increase of z is not equal to the increase of R_G for TriMule. According to literature,[30] the accuracy of TriMule is maintained in workspace of x = [−400 mm, 400 mm], y = [−600 mm, 300 mm] within the

Figure 13. R_G distribution of TriMule within the plane of $z = 1200$ mm: (a) spatial distribution and (b) contour lines.
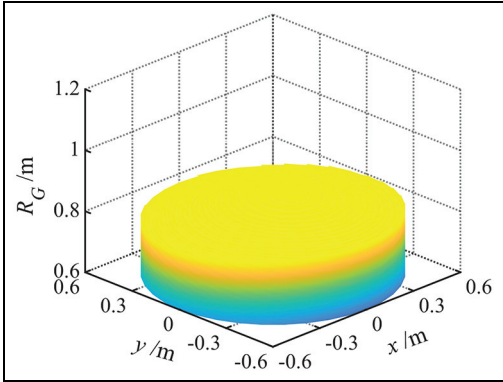
Figure 14. Optimal workspace based on R_G.

plane of z = 800 mm. As the spatial correspondence, the value of R_G can be set as 0.26, to obtain the optimal performance space of TriMule in the whole workspace, as shown in Figure 14.

R_G value choice for design and optimization of manipulator

In the process of robot design and optimization, there are many traditional constraint variables such as kinematics constraints, force constraints,[31] dimensional constraints, pressure angle constraints,[32] and dynamic characteristics constraints.[33] However, R_G can be introduced instead of kinematics and dynamic constraints at the same time, which will effectively constrain the performance of the robot. Meanwhile, R_G can be utilized for the trajectory optimization constraints of manipulator.

If there is the constraint as

$$R_G < constant \tag{37}$$

Where, the *constant* denotes the upper boundary of R_G.

Predictably, κ, dimensional parameters (D_i) and f_1 will be constrained within the limits

$$R_G(\kappa; D_i; f_1) < constant \tag{38}$$

In conclusion, R_G is a convenient and fast performance evaluation method, which can be well applied to the design, optimization, and application evaluation of the robot.

Conclusions

This article presents a performance evaluation approach of the lower mobility hybrid robot based on the vector of gravity center for rapid evaluation, design, and optimization of the robot. The following conclusions are drawn:

1. A general position vector model of gravity center for the lower mobility hybrid robot in the whole workspace is constructed based on a general inverse kinematic model.
2. A rapid performance evaluation index R_G for cantilever robot based on gravity-center position is proposed, which has high sensitivity on mess distribution.
3. The validity of R_G is verified by comparing with the conditional number and the first natural frequency of 5-DOF hybrid robot. The results indicate that R_G have enough credibility, and it can perform performance evaluation accurately for TriMule. It is proved that the gravity-center position vector is closely related to the performance of the manipulator, which is of great significance.
4. The boundary selection of R_G is discussed, which can be used for design and optimization of lower mobility hybrid robot. If R_G is introduced during design and trajectory optimization, the performance of the robot in the whole workspace will be improved.

The line distributions between the conditional number, the first natural frequency, and R_G have been presented. Further work needs to be carried out to perform the relationship between position accuracy, cutting stability, and R_G. These issues, however, deserve to be addressed in separate articles.

Declaration of conflicting interests

ORCID iD

Wentie Niu https://orcid.org/0000-0002-4188-088X

References

1. Neumann K-E. Robot. Patent No. 4,732,525, USA, 1988.
2. Dorries Scharmann Technologie GmbH- SprintZ3 [EB/OL]. [2006-12-10]. Available at: http://www, ds-technologie, de/v3/products/index, php? id = 31& group_id = 9.
3. Chanal H, Duc E and Ray P. A study of the impact of machine tool structure on machining processes. *Int J Mach Tools Manuf* 2006; 46(2): 98–106.
4. Liu H, Huang T, Kecskeméthy A, et al. A generalized approach for computing the transmission index of parallel mechanisms. *Mech Mach Theory* 2014; 74: 245–256.
5. Barnfather JD, Goodfellow MJ and Abram T. A performance evaluation methodology for robotic machine tools used in large volume manufacturing. *Robot Comput Integr Manuf* 2016; 37: 49–56.
6. Joshi S and Tsai L-W. A comparison study of two 3-DOF parallel manipulators: one with three and the other with four supporting legs. *IEEE Trans Rob Autom* 2003; 19(2): 200–209.
7. Zhang D, Wang L and Lang SYT. Parallel kinematic machines: design, analysis and simulation in an integrated virtual environment. *J Mech Design* 2005; 127(4): 580–588.
8. Ma Y, Niu W, Luo Z, et al. Static and dynamic performance evaluation of a 3-DOF spindle head using CAD-CAE integration methodology. *Robot Comput Integr Manuf* 2016; 41: 1–12.
9. Liu H, Huang T, Kecskeméthy A, et al. Force/motion transmissibility analyses of redundantly actuated and overconstrained parallel manipulators. *Mech Mach Theory* 2017; 109: 126–138.
10. Salisbury JK and Craig JJ. Articulated hands: force control and kinematic issues. *Int J Rob Res* 1982; 1(1): 4–17.
11. Yu S, Xie M, Wu H, et al. Design and control of a piezoactuated microfeed mechanism for cell injection. *Int J Adv Manuf Technol* 2019; 105(12): 4941–4952.
12. Gosselin C and Angeles J. A global performance index for the kinematic optimization of robotic manipulators. *J Mech Design: ASME* 1991; 113: 220–226.
13. Huang T, Whitehouse D and Wang J. The local dexterity, optimal architecture and design criteria of parallel machine tools. *CIRP Ann Manuf Technol* 1998; 47(1): 346–350.
14. Huang T, Wang J and Whitehouse D. Design of hexapod-based machine tools with specified orientation capacity and well-conditioned dexterity. In: *Proceedings of the tenth world congress on the theory of machines and mechanism*, vol. 3, Oulu, 20–24 June 1999.
15. Huang T, Wang J and Whitehouse D. Theory and methodology for kinematic design of Gough-Stewart platforms. *Sci China E: Technol Sci* 1999; 42(4): 425.
16. Dong C, Liu H, Yue W, et al. Stiffness modeling and analysis of a novel 5-DOF hybrid robot. *Mech Mach Theory* 2018; 125: 80–93.

17. Dong C, Liu H, Huang T, et al. A screw theory-based semi-analytical approach for elastodynamics of the tricept robot. *J Mech Rob* 2019; 11(3): 031005.
18. Wu L, Wang G, Liu H, et al. An approach for elastodynamic modeling of hybrid robots based on substructure synthesis technique. *Mech Mach Theory* 2018; 123: 124–136.
19. Wang J and Gosselin CM. Static balancing of spatial four-degree-of-freedom parallel mechanisms. *Mech Mach Theory* 2000; 35(4): 563–592.
20. Li Y, Wang J, Liu X, et al. Dynamic performance comparison and counterweight optimization of two 3-DOF parallel manipulators for a new hybrid machine tool. *Mech Mach Theory* 2010; 45(11): 1668–1680.
21. Lin P, Shieh W and Chen D. Design of a gravity-balanced general spatial serial-type manipulator. *J Mech Rob* 2010; 2(3): 031003.
22. Russo A, Sinatra R and Xi F. Static balancing of parallel robots. *Mech Mach Theory* 2005; 40(2): 191–202.
23. Fattah A and Agrawal SK. On the design of reactionless 3-DOF planar parallel mechanisms. *Mech Mach Theory* 2006; 41(1): 70–82.
24. Eckenstein N and Yim M. Modular advantage and kinematic decoupling in gravity compensated robotic systems. *J Mech Rob* 2013; 5(4): 041013.
25. Wu J, Wang J, Wang L, et al. Dynamic analysis and counterweight optimization of the 2-DOF parallel manipulator of a hybrid machine tool. *J Comput Nonlinear Dyn* 2007; 2(4): 344.
26. Ma Y, Zhang J, Dong C, et al. Kinetostatic modelling and gravity compensation of the TriMule robot. In: *IFToMM world congress on mechanism and machine science*, Krakow, June 30–4 July 2019. Cham: Springer.
27. Huang T, Dong C, Liu H, et al. A simple and visually orientated approach for type synthesis of overconstrained 1T2R parallel mechanisms. *Robotica* 2019; 37(7): 1161–1173.
28. Wang C, Zhao Y, Dong C, et al. Kinematic performance comparison of two parallel kinematics machines. In: *IFToMM world congress on mechanism and machine science*, Krakow, June 30–4 July 2019. Cham: Springer.
29. Zhao Y, Wang C, Niu W, et al. Stiffness modeling and analysis of a 3-DOF parallel kinematic machine. In: *IFToMM world congress on mechanism and machine science*, Krakow, June 30–4 July 2019. Cham: Springer.
30. Tian W, Mou M, Yang J, et al. Kinematic calibration of a 5-DOF hybrid kinematic machine tool by considering the ill-posed identification problem using regularisation method. *Robot Comput Integr Manuf* 2019; 60: 49–62.
31. Glorieux E, Franciosa P and Ceglarek D. End-effector design optimisation and multi-robot motion planning for handling compliant parts. *Struct Multidiscipl Optim* 2018; 57(3): 1377–1390.
32. Mei J, Zhang X, Zhang J, et al. Optimization design using a global and comprehensive performance index and angular constraints in a type of parallel manipulator. *Adv Mech Eng* 2018; 10(7): 1687814018787068.
33. Xu H, Xie S, Wang Z, et al. Dynamic optimization design method for high-speed serial industrial robot. In: *Proceedings of the 2018 IEEE international conference on real-time computing and robotics (RCAR)*, Kandima, Maldives, 1–5 August 2018.

Author biographies

Chensheng Wang is a PhD Candidate at Tianjin University, China. And her research interests are dynamics and control of machine tools.

Fang Su is a college lecturer at Shanxi Datong University, China. And her research interests are dynamics and control of machine tools.

Yanqin Zhao is a PhD Candidate at Tianjin University, China. And her research interests are stiffness, dynamics and control of parallel kinematic machines.

Hongda Liu is a PhD Candidate at Tianjin University, China. And her research interests is dynamics of machine tools.

Yonghao Guo is a PhD Candidate at Tianjin University, China. And her research interests is dynamics and control of parallel kinematic machines.

Wentie Niu is an associated professor at School of Mechanical Engineering, Tianjin University, China. His research interests are intelligent agricultural equipments and robots.